Evaluation of Flow Schemes for Near-Neutral Electrolytes in Solar-Fuels Generators

3 authors, including:

Meenesh R. Singh
University of Illinois at Chicago

34 PUBLICATIONS   **435** CITATIONS

Some of the authors of this publication are also working on these related projects:

Electrochemical Reduction of Carbon Dioxide View project

Evaluation of Flow Schemes for Near-Neutral Electrolytes in Solar-Fuels Generators

Meenesh R. Singh,[1,2] Chengxiang Xiang[3,*] and Nathan S. Lewis[3*]

1. *Joint Center for Artificial Photosynthesis, Lawrence Berkeley National Laboratory, Berkeley CA 94720*

2. *Department of Chemical Engineering, University of Illinois at Chicago, Chicago, IL 60607*

3. *Division of Chemistry and Chemical Engineering, 210 Noyes Laboratory, 127-72, California Institute of Technology, Pasadena, CA 91125*

*To whom correspondence should be addressed: cxx@caltech.edu, nslewis@caltech.edu

ABSTRACT

The electrochemical performance of three different types of membrane-containing electrolyte-flow schemes for solar-driven water splitting has been studied quantitatively using 1-dimensional and 2-dimensional multi-physics models. The three schemes include a recirculation scheme with a well-mixed bulk electrolyte, a recirculation scheme with laminar flow fields, and a fresh-feed scheme with laminar flow fields. The Nernstian potential loss associated with pH gradients at the electrode surfaces, the resistive loss between the cathode and anode, the product-gas crossovers, and the required pumping energy in all three schemes have been evaluated as a function of the operational current density, the flow rates for the electrolyte, and the physical dimensions of the devices. The trade-offs in the voltage loss, safety considerations, and energy inputs from the balance-of-systems required to produce a practical device have been evaluated and compared to membrane-free devices as well as to devices that operate at extreme pH values.

1.   INTRODUCTION

Strongly alkaline or strongly acidic electrolytes typically are used in commercial water-electrolysis systems because such electrolytes allow maximally efficient operation and offer engineering advantages such as facilitating the safe collection of the H_2 product under pressure. [1, 2, 3] However, when employed in integrated solar-driven water-splitting systems that consist of a photovoltaic or photoelectrochemical cell in direct contact with the electrolyte, strongly alkaline or acidic media generally enhance the tendency of the photoactive semiconductor materials to participate in deleterious dark and/or photocorrosion processes. For instance, GaAs passivates anodically between pH 4 and 10, but due to the solubility of the amphoteric oxides, GaAs undergoes active photocorrosion in acidic (pH <4) or alkaline (pH > 10) media.[4] One approach to circumvent this hurdle is to discover materials, such as new metal oxides, that are inherently stable under these conditions.[5] An alternative approach involves the development of new protection schemes, in combination with active electrocatalysts, that are amenable to operation in a highly acidic or alkaline environment.[6] Advances along the latter approach have been reported recently, such as the demonstration of enhanced stability of a series of technologically important semiconducting photoanodes, including Si, GaAs, InP, CdTe, $BiVO_4$, and amorphous hydrogenated Si, either by use of "leaky" films of TiO_2 deposited by atomic-layer deposition, in conjunction with islands of a Ni(OH)/oxide electrocatalyst,[7] and/or by the use of reactive sputtering to prepare conductive, transparent, stable, catalytic, protective NiO_x films on a variety of passivating semiconducting photoanode surfaces.[8]

Significant attention has also been devoted to the development of electrocatalysts[9-12] and electrolysis systems that can operate at near-neutral pH.[13-15] Specifically, a fully integrated membrane-free solar-driven water-splitting system has been investigated and its behavior

3

compared in detail to a multi-physics model as well as to that of an identical system that additionally incorporated an ion-exchange membrane.[13] The membrane-free device exhibited significant product crossover between the cathode and anode compartments, with up to 40% $H_2(g)$ in the cathode chamber. Use of a membrane led to electrodialysis of the buffer species and resulted in very low current densities, and concomitantly low efficiencies, under steady-state operation in the passive system.[13] In addition, modeling of a one-dimensional solar-driven water-splitting cell with membrane separators showed that significant Nernstian potential losses associated with large pH gradients (more than 6 pH units) at the surface of the electrodes were present even at low operating current densities (~ 1 mA cm^{-2}).[14] Hence, such near-neutral pH, passive, solar-driven water-splitting systems are fundamentally limited in efficiency and/or co-evolve explosive mixtures of $H_2(g)$ and $O_2(g)$ in the presence of active catalysts for recombination of the gaseous products.

As a consequence of these limitations, one approach that has been proposed to prevent a continual increase in electrodialysis of the electrolyte, while also arresting the growth of a pH gradient, involves active system designs that recirculate the electrolyte, at a controlled flow rate, between the anolyte and catholyte.[16] Such a system recently has been constructed and operated at steady state for extended periods of time.[16] However, a quantitative understanding of the transport loss, and computational models that explicitly include flow schemes, have not been developed. For instance, the energy losses associated with the operation of such a system, as well as the gas crossover and the ability to withstand pressure differentials to facilitate beneficial collection, in a safe fashion, of the $H_2(g)$, have not been evaluated. The magnitude and spatial distribution of any residual pH gradients and associated concentration overpotentials have also not been treated analytically for the liquid-recirculating electrolysis system.

We describe herein the use of multi-physics modeling and simulation to evaluate these key performance features of a solar-driven water-splitting system with a recirculating, near-neutral pH electrolyte. The hydrogen-evolution reaction (HER) and the oxygen-evolution reaction (OER) were explicitly employed in the simulation, but the modeling results are also generally applicable a CO_2 reduction cathode, because each electron involved in CO_2 reduction also consumes a proton during the reaction and thus produces the same polarization losses in the electrolyte as those produced by a cathode instead effecting the HER. The multi-physics model has been validated previously and has been used to assess in detail the design rules for a variety of solar-fuels generators, including 1-D and 2-D fixed-focus concentrator systems as well as other generic system designs.[13, 14] The system designs evaluated to date have exploited passive transport mechanisms, including mass transport by diffusion, migration and natural or forced convection. Herein we have explicitly included active recirculation or flow pathways to allow for assessment of the behavior of such systems. We have specifically assessed the trade-offs that accompany this suite of design approaches, including gas crossover, resistance drops, pH gradients, electrodialysis of the electrolyte, and the intrinsic safety of the system. Additionally we provide comparisons and modeling insights to experimentally demonstrated solar-driven water-splitting systems.[13, 15, 16] This work provides the design principles for efficient operation of 1D/2D photoelectrochemical flow cells with active convection, including a detailed analysis of the polarization losses, gas crossover, and pumping energy as a function of current density, flow rates and cell dimensions in various flow-cell configurations.

2. MODELING

2.1 Cell design

Figure 1 illustrates three different schemes of active transport in a one-dimensional (1-D) planar model of a photoelectrochemical (PEC) cell. Although the cells in Figure 1 are two-dimensional (2-D), the transport of species and their concentration distribution does not vary in the direction along the length of the electrode and only varies along in the direction that is perpendicular to the electrodes. Therefore, this situation effectively constitutes 1-D transport, and hence these cells are referred to as 1-D cells. These cells were used to analyze the transport of species in the electrolyte, as well as to evaluate the effect of electrolyte recirculation on the polarization losses and intermixing of product gases in such systems. Scheme A and Scheme B in Figure 1 involve external flow (also called recirculation) between the anolyte and the catholyte at a controlled flow rate. A well-mixed electrolyte, in which the bulk electrolyte outside the boundary layer has no concentration gradient, was assumed for Scheme A, and the magnitude of convective mixing was parameterized by specifying the thickness of the hydrodynamic boundary layer. A velocity field with a symmetric parabolic profile corresponding to laminar flow in the cathode and anode chambers, with the inlet located at the midpoint of each chamber, was assumed for Scheme B. Scheme C is based on a continuous feed of fresh electrolyte to the anode and cathode chambers. A two-dimensional (2-D) PEC cell configuration with the electrolyte in laminar flow was also used for comparative evaluation. In the 1-D model, the membrane thickness was set to 200 µm and the physical spacing between the cathode and the anode was treated as a variable. In the 2-D model, the width of the photoelectrode was set to 18 mm such that the mean ionic path length is similar to 1-D cell, the width of the membrane was set to 1 mm (10% of the half-cell width) which is optimal of 2-D PEC[1], the height of the photoelectrode was set to 100 µm, and the height of the electrolyte was 4 mm which ensures flow-field to be similar to 1-D cell.

In the 1-D simulation, the transport loss of the system is only a function of the electrolyte properties, cell dimensions, flow rates and current densities and is independent of the detailed electrocatalytic properties of the cathode and anode materials including the exchange current densities and the transfer coefficients. This study has focused on the effects of the operational current densities, flow rates and cell dimensions and assumed a phosphate buffer electrolyte at a total buffer capability of 1.0 M. Figure S1 shows that the transport loss exhibited a weak dependence on the diffusion coefficients of the dissolved species in the range of 1X to 4X, because the polarization losses are logarithmically dependent on the concentration gradient, which for constant flux varies linearly with the diffusion coefficient. Moreover, the diffusion coefficients are uniform and do not vary spatially in the dilute electrolytes (< 1 mol%).

The physical properties of the phosphate buffer electrolyte such as diffusion coefficients and gas solubility, and the kinetic properties of HER and OER such as exchange current density and transfer coefficients, are tabulated in the Supporting Information (SI).

2.2   Species transport in the electrolyte and in the membrane separator

Established electrochemical relationships, specifically, the Nernst-Planck equation, were used to describe the flux of species in the electrolyte, including diffusion, migration, convection and bulk reactions of water and buffer dissociation.[13, 17] Ionic species (protons, hydroxides, sodium, dihydrogen phosphate and monohydrogen phosphate) and neutral species (water, and dissolved hydrogen and oxygen) were included in the model. The initial electrolyte composition was set to pH = 7.21 by use of 0.5 M NaH_2PO_4(aq) and 0.5 M Na_2HPO_4(aq). We have previously shown the effect of buffer concentration on the polarization losses and found that 0.5 M concentration is sufficient to buffer the electrodes at 10 mA cm^{-2} of current density.

The simulation conditions for Scheme A corresponded to the recirculation cell of Modestino et al,[16] in which a well-mixed anolyte and catholyte were separated by a cation-exchange membrane (Nafion) with an estimated hydrodynamic boundary-layer thickness of 100 μm.[16]   Figure S3 shows the change in the polarization loss with increasing boundary-layer

thickness in Scheme A. In Scheme A, the transport of species to the surface of the electrode was mainly governed by the active stirring in each chamber, so at low flow rates (< 44 µl cm^{-2} min^{-1}) the thickness of the hydrodynamic boundary layer was assumed to be independent of the flow rate of the recirculating electrolyte. Perfect mixing, with no diffusional resistance of solution species, was assumed beyond the hydrodynamic boundary layer in the bulk solution, to account for the stirring in the cell. The polarization losses were calculated as a function of the operational current densities for each of five different rates of recirculation flow (0, 0.7, 3.6, 7.3, 14.6, and 43.8 µl cm^{-2} min^{-1}).

Scheme B and Scheme C have fully developed countercurrent laminar flows in the anode and cathode chambers. The systems depicted in Scheme B and C have laminar flow, because the Reynolds number is < 82 for flowrates of < 7290 µL cm^{-2} min^{-1}, which is much smaller than the critical Re = 2300 for the transition to turbulent flow. Scheme B uses electrolytes from the opposite reaction chambers, whereas Scheme C uses a fresh-feed electrolyte with the initial electrolyte compositions. For both schemes, the polarization losses as a function of the operating current densities were simulated at five different recirculation flow rates (0, 7.3, 36.5, 73, 365, and 730 µl cm^{-2} min^{-1} for Scheme B and 0, 70, 370, 1460, 3650, and 7290 µl cm^{-2} min^{-1} for Scheme C).

The cation-exchange membrane (CEM) was modeled as a polymeric electrolyte in which the diffusion coefficients of anions and cations were reduced by a factor of 10^{-2} and 10^{-1}, respectively, relative to their corresponding values in the bulk solution.[18-20] A fixed 1.0 M positive background charge was assumed in the cation-exchange membrane. The charge separation and Donnan potential at membrane/electrolyte interfaces were also considered in the model.

The energy loss due to the pumping of the electrolyte was calculated using the equation for ideal hydraulic power:

$$P_h = 6 \times 10^6 \, q \, \rho \, g \, h \tag{1}$$

where P_h is the hydraulic power in W m^{-2} of electrode area, q is the flow rate in µl cm^{-2} min^{-1}, ρ is the density of electrolyte in kg m^{-3}, g is acceleration due to gravity in m s^{-2}, and h is the total head loss in m. The total head loss is the sum of i) the head loss in the electrolyte chambers, and ii) the head loss at the entrance and exit of electrolyte chambers due to expansion and contraction of fluid. Assuming that the head loss is the same in the anolyte and catholyte chambers, the expression for total head loss is therefore:

$$h = 2\left(h_{electrolyte} + h_{entrance} + h_{exit}\right)$$
$$= \frac{V^2}{g}\left(\frac{\alpha H_{el}\left(W_{el}+D_{el}\right)}{2W_{el}D_{el}} + \xi\left(\frac{W_{el}D_{el}}{A_d}-1\right)^2 + \left(\frac{1}{\mu}-1\right)^2\left(\frac{W_{el}D_{el}}{A_d}\right)^2\right) \tag{2}$$

where $h_{electrolyte}$ is the head loss in the electrolyte chambers due to friction, $h_{entrance}$ is the head loss at the entrance of the electrolyte chambers due to sudden expansion of fluid, h_{exit} is the head loss at the exit of the electrolyte chambers due to sudden contraction of fluid, V is the mean velocity of fluid in the electrolyte chambers, α is the friction coefficient, H_{el} is the height of the electrode along the direction of flow, W_{el} is the width of the electrolyte, which is also the distance between membrane and electrode, D_{el} is the depth of the electrolyte/electrode, ξ is the coefficient of expansion, A_d is the area of conduit connecting external reservoirs to the electrode chambers, and μ is the coefficient of contraction. The head loss at the entrance and exit was modeled using the Borda-Carnot equation, in which the coefficient of expansion is close to 1 and the coefficient of contraction is empirically obtained as:[21]

$$\mu = 0.63 + 0.37\left(\frac{A_d}{W_{el}D_{el}}\right)^3 \tag{3}$$

The coefficient of friction for a rectangular conduit of aspect ratio > 8 is given as:[21]

$$\alpha = \frac{82.32}{Re} \tag{4}$$

where Re is the Reynolds number.

In addition to the assumptions given above, some of the primary assumptions of the model are – i) the ionic flux expression is given by dilute solution theory, ii) the electrolyte entering the cell has a fully developed laminar profile, iii) the cell operates isothermally at room

temperature, iv) the boundary layer thickness of the cell in Scheme-A is 100 µm, and is independent of the recirculation flow rate, and iv) the acid-base reactions in the electrolyte are sufficiently rapid to allow for instantaneous attainment of equilibrium.

2.3 Governing relations for polarization losses

The total voltage requirement $\left(\Delta\phi_{cell}\right)$ for an electrochemical cell is the sum of the equilibrium potential $\left(E_0\right)$, kinetic overpotentials $\left(\eta\right)$, solution potential losses $\left(\Delta\phi_{solution}\right)$, and the Nernstian potential losses associated with pH gradients at the surface of the electrodes $\left(\Delta\phi_{pH\ gradients}\right)$:

$$\Delta\phi_{cell} = E_0 + \eta_{OER} - \eta_{HER} + \Delta\phi_{solution} + \Delta\phi_{pH\ gradient} \tag{5}$$

The equilibrium potential is assumed to be only dependent on the pH. The Nernst equation clearly indicates that the kinetic overpotential $\eta = V - E^o$ is also a function of pH. We have assumed that the exchange current densities for the OER on IrO_x and for the HER on Pt are independent of pH. Although the electrode kinetics may be dependent on pH,[22] the assumptions and specific expressions of the OER and HER kinetics do not affect the polarization loss of the system, which is only dependent on the electrolyte properties, cell dimension, flow rates and the operating current density. The solution losses, $\left(\Delta\phi_{solution}\right)$, are the sum of the ohmic resistance loss (first term) and the electrodialysis loss (second term). These losses can be expressed as:

$$\Delta\phi_{solution} = \int \frac{J}{\kappa}dx + \sum_i \int \frac{Fz_i D_i \nabla c_i}{\kappa}dx \tag{6}$$

where ϕ is the electric potential, κ is the conductivity of the electrolyte, J is the current density, x is distance along the axis of the 1-D model, F is Faraday's constant, z is the charge number, D_i is the diffusion coefficient and c_i is the molar concentration of the ith species. The distribution of the ionic conductivity, $\kappa(x)$, and of the species concentrations, $c_i(x)$, obtained from COMSOL Multiphysics were used in the above equations to calculate the ohmic and

electrodialysis losses of the system. The additional computational details are provided in the SI. The potential loss due to the pH gradient was obtained by the Nernstian term:

$$\Delta\phi_{\text{pH gradient}} = 2.303\frac{RT}{F}\left(\text{pH}_{\text{cathode}} - \text{pH}_{\text{anode}}\right) \tag{7}$$

where R is the gas constant, and T is the absolute temperature. The polarization loss is a sum of pH gradient and the solution losses. In the case of 2-D PEC, the average value of the pH gradient as well as the average of the transport losses at the electrolyte-electrode interface along the electrode dimensions were used to approximate these parameters.

3.   RESULTS

3.1   One-Dimensional cell model

Figures 2a and b show the steady-state polarization loss as a function of the operating current density (polarization curve) of the recirculation cells in Scheme A and Scheme B, respectively. Regardless of the flow conditions (stirred or laminar flow) of the electrolyte, for a fixed current density, the polarization loss decreased as the recirculation flow rate increased. The limiting current density without recirculation was < 0.37 mA cm^{-2}, which is comparable to the value of the current density that has been observed experimentally in such a system.[16] Figure 2a shows that, in Scheme-A, a recirculation flow rate > 14.6 µl cm^{-2} min^{-1} is required to obtain current densities > 10 mA cm^{-2} while limiting the polarization losses to < 100 mV. A recirculation flow rate of 43.8 µl cm^{-2} min^{-1} is sufficient to reach ~18 mA cm^{-2} of current density in Scheme A while still keeping the polarization losses to < 200 mV.

An analogous, well-mixed recirculating device that contained stir bars inside the cell has been constructed experimentally. At the reported recirculation flow rate of 44 µl cm^{-2} min^{-1} and an operational current density of ~2.3 mA cm^{-2}, during steady-state operation the modeling suggested a total polarization loss of ~20 mV, and a pH gradient between the surface of the cathode and anode of ~0.19. The majority of the potential loss in the reported system resulted from kinetic overpotentials of HER and OER in the near-neutral pH electrolyte.

Figure 2b shows that an order of magnitude higher recirculation flow rate is required in Scheme B, due to the imperfect mixing, to attain similar current densities as those in Scheme A. For example, in Scheme B a recirculation flow rate of 730 µl cm^{-2} min^{-1} is required to obtain ~18

mA cm^{-2} of current density. Additionally, the polarization curve in Scheme B exhibited higher slopes relative to the behavior of the system depicted in Scheme A.

Figure 2c shows polarization curves for a flow cell with a fully-developed, counter-current, laminar flow of a fresh feed electrolyte (Scheme C). An order of magnitude higher flow rate is required in Scheme C to obtain similar current densities to those produced by Scheme B. The polarization curves in Figures 2b and 2c show the appearance of two plateaus,[14] and the curves have mutually similar slopes.

Figure 3a shows the local pH at the surface of the cathode and anode as a function of flow rate for each of the three Schemes, at an operational current density of 10 mA cm^{-2}. The electrode pH started to deviate from the bulk pH value for flow rates of < 14 µl cm^{-2} min^{-1} for Scheme A, < 290 µl cm^{-2} min^{-1} for Scheme B, and < 1460 µl cm^{-2} min^{-1} for Scheme C. A steep increase in the local pH near the cathode to pH 12, and a steep decrease in the local pH near the anode to pH 2, was observed below these specified minimum flow rates. For three different schemes, Figure 3b shows the polarization loss as a function of the flow rate, at 10 mA cm^{-2} of operational current density. To keep the overall polarization loss < 200 mV, the required minimum a flow rates were 12 µl cm^{-2} min^{-1} for Scheme A, 340 µl cm^{-2} min^{-1} for Scheme B, and >3000 µl cm^{-2} min^{-1} for Scheme C.

Figure 4a shows the local pH at the surface of the cathode and anode as a function of the physical spacing between the electrodes, at an operational current density of 10 mA cm^{-2} and at a flow rate of 730 µl cm^{-2} min^{-1}. For Scheme A and Scheme B, when the electrode spacing was less than 20 mm, the local pH at the electrode surfaces exhibited relatively small deviations from the bulk pH values. In contrast, for Scheme C, the local pH at the electrode surfaces showed a rapid change when the electrode spacing increased beyond 2 mm. Figure 4b shows the total polarization losses as a function of the electrode spacing at an operational current density of 10 mA cm^{-2} with a flow rate of 730 µl cm^{-2} min^{-1}. For Scheme A and Scheme B, the increase in the total polarization loss as a function of the increased path length for ionic transport was primarily due to the increased resistive loss in the system. The ionic conductivity of the electrolytes was insensitive to the convective mixing conditions, hence Scheme A and Scheme B exhibited similar total polarization losses. At large electrode spacings, the resistive losses were the dominant factor for Scheme A and Scheme B. In contrast, for Scheme C, the Nernstian loss

associated with the pH gradients at the electrode surface was the primary cause of the rapid increase of the polarization loss in the system. To maintain polarization losses of < 200 mV, the maximum allowable electrode spacing was 10.4 mm for Scheme A, 10.8 mm for Scheme B, and 3.5 mm for Scheme C.

3.2   Two-dimensional cell model

Figure 5a shows the polarization curves for the 1D and the 2D PEC flow cells, respectively, operating at 7300 µl cm^{-2} min^{-1} of fresh electrolyte feed. At an operating current density of 10 mA cm^{-2}, the 2D PEC cell had an additional 140 mV of potential loss as compared to the 1D PEC cell, primarily resulting from the longer pathways for the electrolyte transport that resulted in larger resistive losses in the system. The polarization losses for the 1D PEC cell increased rapidly with increasing current density, due to the local pH gradients (Figure 2c), and became comparable to the polarization loss of the 2D PEC cell at an operational current density of 18 mA cm^{-2}.   At still larger current densities, the 1D PEC was completely polarized whereas the 2D PEC cell still maintained a near-neutral pH condition near the electrode surfaces. The linear behavior of the polarization curve for the 2D PEC cell indicated that at a flow rate of 7300 µl cm^{-2} min^{-1}, the polarization loss is governed by the resistive loss in the system, and the local pH at the electrode surface did not deviate from its bulk value even at an operating current density of 18 mA cm^{-2}.   Figure 5b shows the current distribution in the 2D PEC cell at an operational current density of 18 mA cm^{-2}.   A non-uniform spatial distribution of the current density was observed.   Figure 5c and 5d show the potential distribution, pH distribution and velocity field for a 2D PEC cell operating at 18 mA cm^{-2} of current density. The potential losses were maximized at the center and minimized at the edges of the 2D PEC cell. However, the pH difference reached a maximum at the edges and was minimized at the center of the electrodes.

4.   DISCUSSION

4.1 Comparison among three recirculation configurations

Among the three configurations investigated, the well-mixed recirculation cell, Scheme A, yielded the lowest polarization loss at a given recirculation flow rate. Turbulent mixing is often required to achieve the mixing conditions assumed to prevail in Scheme A. For instance, the well-mixed condition was produced by placing stir bars in the cathode and anode chambers.[16] The scale up of such systems to large areas in the field seems challenging to implement in practice. Alternatively, a laminar flow between electrode and membrane can be used to mix and recirculate the anolyte and catholyte in the system. To obtain mutually similar current densities, the laminar recirculation cells required at least 10 times higher flow rates than the stirred, well-mixed recirculation cells (Figure 2a and 2b). Inefficient mixing in the laminar flow produces a high ionic resistance in such configurations, so for a given flow rate the polarization loss in Figure 2b is higher than that in Figure 2a.

Both Scheme A and Scheme B used the electrolytes from the opposite reaction chamber as the feed electrolyte. Specifically, the anolyte, with a lower pH value and lower salt concentration, was fed into catholyte, which had a higher pH value and higher salt concentrations, to increase the effectiveness of the mixing in the recirculation configurations. By comparison, Scheme C used a fresh electrolyte feed having the initial electrolyte composition, and required significantly higher flow rates to achieve the attainable operational current density. A similar strategy has been used in a membrane-less microfluidic electrolyzer, in which fresh electrolytes were continuously fed into the cell with the product bubbles separated by the flow fields.[15] Such a flow scheme has been shown to require the operational flow rates of at least 1900 $\mu l\ cm^{-2}\ min^{-1}$ to sustain > 10 mA cm^{-2} current density with marginal losses due to pH gradients.[15] Figure 2c shows that the minimum flow rate required to support >10 mA cm^{-2} of current density is 1460 $\mu l\ cm^{-2}\ min^{-1}$, and shows that the pH gradients decrease to a negligible value as the flow rate approaches the reported value of 1900 $\mu l\ cm^{-2}\ min^{-1}$. Electrodialysis of the electrolytes store electrochemical energy as a concentration gradient between the catholyte and anolyte, and that concentration gradient was unexploited in Scheme C. A well-stirred fresh electrolyte, similar to Scheme A, will require flowrates larger than ~14.6 $\mu l\ cm^{-2}\ min^{-1}$ to support 10 mA cm^{-2} of current density, as it does not utilize the electrochemical energy stored in the concentration

gradients. In principle, additional engineering approaches could be taken to improve the efficiency by using the electrochemical energy stored in the concentration gradients of the catholyte and anolyte in the system. For instance, reservoirs of catholyte and anolyte could allow for degassing of dissolved product gases, and after significant concentration gradients are produced, the catholyte and anolyte could be switched with the resulting the pH differential between the two electrolytes favoring the water-splitting reaction in the system. Further improvement in the energy efficiency could be obtained by using serpentine channels to achieve higher flow rates, lower boundary layer thickness and hence lower polarization losses.[23]

4.2 Energy balance in the recirculation system

The preferential transport of sodium ions from the anolyte to catholyte causes the sodium salt to accumulate in the catholyte during water electrolysis, hence limiting the attainable current density to < 0.37 mA cm^{-2} in steady-state operation with a near-neutral pH electrolyte.[16] The recirculation schemes continuously transfer salt accumulated in the catholyte to the anolyte. In the current cell configuration, the volumetric flow rate of sodium through Nafion is 4.2 µl cm^{-2} min^{-1} at 10 mA cm^{-2} of current density. However, all three schemes require significantly higher flow rates (e.g. >14.6 µl cm^{-2} min^{-1} for Scheme A, >365 µl cm^{-2} min^{-1} for Scheme B, and >3650 µl cm^{-2} min^{-1} for Scheme C) to maintain the polarization losses < 200 mV at 10 mA cm^{-2} and to maintain a steady-state electrolyte composition, due to ineffective mixing. The additional energy required to pump the electrolyte was calculated to be 7.16×10^{-9} W m^{-2} for Scheme A, 6.14×10^{-5} W m^{-2} for Scheme B, and 5.96×10^{-2} W m^{-2} for Scheme C, which are negligible relative to the solar insolation power.

4.3 Safety considerations

The recirculation cells in Scheme A and Scheme B could produce flammable mixtures at higher flow rates if the inlet electrolytes are not properly degassed. With a 200 µm thick Nafion membrane, the calculated crossover rates for $O_2(g)$ and $H_2(g)$ are 0.54 % (an equivalent current density of 0.158 mA cm^{-2}) and 1.6 % (an equivalent current density of 0.054 mA cm^{-2}), respectively, without any active flow in the system (see Figure S1 in Supplementary Information). Without any degassing process, the O_2-saturated anolyte or the H_2-saturated catholyte will enter the opposite reaction chamber. Hence crossover of hydrogen and oxygen increases as a function of the recirculation flow rate. To keep the product-gas mixture below the

15

flammable limit (4 volume percent of hydrogen in oxygen),[24] the recirculation flow rate needs to be limited to < 80 µl cm^{-2} min^{-1} (See Figure S1 in the Supporting Information). Due to the effective mixing, Scheme A allows efficient operation of the cell even at low flow rates, but such low flow rates, bounded by safety concerns, in turn would result in high polarization losses in Schemes B and C and thus inefficient electrolyzer systems (Figure 2b and 2c).

The degassing of the electrolyte before recirculation, as mentioned above, reduces the gas crossover while still utilizing the concentration polarization. The critical flow rate required to produce flammable mixtures after 90% of degassing is 360 µl cm^{-2} min^{-1}, which enables Scheme B to support 10 mA cm^{-2} of current density at ~200 mV of polarization loss.

4.4   Comparison between the 1D and 2D cell configurations.

In a 2D PEC, back-to-back cell configuration based on a planar, impermeable tandem- or triple-junction semiconductor device,[13, 25, 26] the ionic transport between the cathode surface and the anode surfaces must occur around the edges of the light-absorbing material.   The electrochemical engineering-design principles of this type of system have been assessed in detail previously.[1] Forced convection due to laminar flow significantly decreased the pH gradients at the electrode surface relative to a passive system (Figure 5d).

Figure 5a shows the polarization curves for 1D and 2D PEC flow cells operating with a fresh feed of phosphate buffer at 7300 µl cm^{-2} min^{-1}. The average polarization loss at 10 mA cm^{-2} in a 2D cell is 140 mV higher than the 1D cell, which also indicates that the pH changes are higher especially at the edges of the photoelectrode. In a 1D PEC cell, the ions must travel across all of the lamellae of fluid, whereas in a 2D PEC cell, ions close to the edge of photoelectrodes can transport directly across the membrane without seeing lamellae of fluid. Therefore, the 2D PEC cell can support higher current densities than the 1D PEC cell while still maintaining close to near-neutral pH values adjacent to the electrode surfaces.

The 1D analysis shown in Figure 4 allows for a qualitative assessment of the effect of electrode and cell dimensions on the performance of the 2D PEC cell. For either the 1D or 2D PEC cells, when the physical spacing between the cathode and anode is large, the total

polarization loss associated with the resistive loss will eventually limit the cell performance. For instance, for Scheme B and Scheme C, minimal pH gradients developed at the electrode surfaces, but the resistive loss reached >200 mV at an electrode spacing of 10.4 mm (Figure 4b). A similar trend is expected in the 2D PEC cell in either the recirculation or flow configurations. The flow of electrolyte in these conditions has a minimal effect on the conductivity of the electrolyte, so the resistive loss in the recirculation or flow system is expected to be very similar to that in a passive system, for which the allowable physical dimensions of the cell have been previously evaluated.[1]

4.5 Comparison between electrolyte flow devices, membrane-free devices, and devices that operate at extreme pHs

Figure 6 illustrates three types of PEC devices: a recirculation system with near-neutral pH electrolytes with a membrane separator (Fig. 6a), a passive transport system at near-neutral pH without a membrane separator (Fig. 6b), and a passive transport system at extreme pH with a membrane separator (Fig. 6c). Efficient mixing of the catholyte and anolyte can be achieved, in principle, at sufficiently high flow rates by electrolyte flow schemes (Fig. 6a) or without any electrolyte flow schemes, by passive diffusion and natural convection, in membrane-free devices (Fig. 6b) provided that the critical path-length is sufficiently short between the cathode and anode. Efficient proton transport or hydroxide transport between the cathode and anode, with minimal polarization losses, can also be readily achieved at extreme pHs in a passive system by the use of cation exchange membranes or anion exchange membranes (Fig. 6c).[27] With small PEC electrode dimensions, all three devices could potentially yield low ohmic resistive losses in the electrolyte as well as low voltage losses associated with pH gradients and electrodialysis.

In terms of the ionic transport and the fluid, the recirculation system (Fig. 6a) and the membrane-free, passive transport system (Fig. 6b) are equivalent in achieving catholyte and anolyte mixing that minimizes the steady-state electrodialysis of the cell solutions. The membrane-containing recirculation schemes (Fig. 6a) could potentially prevent local product gas

crossover and recombination currents under spatially and temporally varying operational temperatures and illumination conditions, but require external degassing of the recirculating electrolyte. The degassing process needs to ensure that the $H_2(g)/O_2(g)$ gas mixture ratio in either the cathode or anode chamber is outside of the flammable limit, for a wide dynamic range of hydrogen and oxygen production rates, throughout a day. In contrast, for the passive transport of electrolytes and large electrode dimensions that act as gas-impermeable barriers, significant product-gas crossovers have been observed experimentally even in devices with small electrode areal fractions.[28] To facilitate electrolyte mixing, a significant decrease in the electrode dimension is necessary, and in devices with small electrode dimensions, diffusive and convective crossovers would significantly increase the recombination currents and compromise the safety of the device.

Relative to the passive transport devices that operate at extreme pHs (Fig. 6c), the membrane-containing electrolyte-flow devices that operate at near-neutral pH significantly relax the requirements on light-absorber materials to yield stable operation in the electrolyte. However, most active electrocatalysts for OER and HER operate at extreme pHs.[29] For instance, at near-neutral pH the available OER catalysts exhibit significant overpotential losses (>400 mV at 10 mA cm^{-2}), compared to operation in alkaline electrolytes. Both types of devices could produce small voltage losses resulting from the polarization loss in the electrolyte and the in membrane. Other relevant factors for practical implementation of flow-cells are discussed in the SI.

5.   CONCLUSIONS

Numerical modeling indicated that recirculation could significantly reduce the Nernstian potential loss associated with pH gradients at the surface of the electrodes, and could minimize electrodialysis of the bulk electrolytes in the cell. At sufficiently high flow rates, low voltage losses can be achieved in all three schemes considered, and the resistive loss between the cathode and anode electrode becomes the dominant factor as the increasing electrode spacing increases. The required additional pumping energy only constituted a small fraction of the overall energy that was converted and stored in the system. Relative to systems that operate at extreme pHs, degassing systems and engineering challenges are involved with the production of $H_2(g)$ at elevated pressure in a flow cell system relative to a passive system that operates at extreme pH values.

6. ACKNOWLEDGEMENTS

REFERENCES

1.   S. Haussener, C. Xiang, J. M. Spurgeon, S. Ardo, N. S. Lewis and A. Z. Weber, *Energy & Environmental Science*, 2012, **5**, 9922-9935.
2.   A. Berger, R. Segalman and J. Newman, *Energy & Environmental Science*, 2014, **7**, 1468-1476.
3.   K. Zeng and D. Zhang, *Progress in Energy and Combustion Science*, 2010, **36**, 307-326.
4.   S.-M. Park and M. E. Barber, *Journal of Electroanalytical Chemistry and Interfacial Electrochemistry*, 1979, **99**, 67-75.
5.   S. Chen and L.-W. Wang, *Chemistry of Materials*, 2012, **24**, 3659-3666.
6.   S. Hu, M. R. Shaner, J. A. Beardslee, M. Lichterman, B. S. Brunschwig and N. S. Lewis, *Science*, 2014, **344**, 1005-1009.
7.   S. Hu, N. S. Lewis, J. W. Ager, J. Yang, J. R. McKone and N. C. Strandwitz, *The Journal of Physical Chemistry C*, 2015, **119**, 24201-24228.
8.   K. Sun, F. H. Saadi, M. F. Lichterman, W. G. Hale, H.-P. Wang, X. Zhou, N. T. Plymale, S. T. Omelchenko, J.-H. He and K. M. Papadantonakis, *Proceedings of the National Academy of Sciences*, 2015, **112**, 3612-3617.
9.   A. Minguzzi, F.-R. F. Fan, A. Vertova, S. Rondinini and A. J. Bard, *Chem. Sci.*, 2012, **3**, 217-229.
10.   D. K. Bediako, B. Lassalle-Kaiser, Y. Surendranath, J. Yano, V. K. Yachandra and D. G. Nocera, *J. Am. Chem. Soc.*, 2012, **134**, 6801-6809.
11.   M. W. Kanan, Y. Surendranath and D. G. Nocera, *Chem. Soc. Rev.*, 2009, **38**, 109-114.
12.   M. Cabán-Acevedo, M. L. Stone, J. Schmidt, J. G. Thomas, Q. Ding, H.-C. Chang, M.-L. Tsai, J.-H. He and S. Jin, *Nature Materials*, 2015.
13.   J. Jin, K. Walczak, M. R. Singh, C. Karp, N. S. Lewis and C. Xiang, *Energy & Environmental Science*, 2014, **7**, 3371-3380.
14.   M. R. Singh, K. Papadantonakis, C. Xiang and N. S. Lewis, *Energy & Environmental Science*, 2015, **8**, 2760-2767.
15.   S. M. H. Hashemi, M. A. Modestino and D. Psaltis, *Energy & Environmental Science*, 2015, **8**, 2003-2009.
16.   M. A. Modestino, K. A. Walczak, A. Berger, C. M. Evans, S. Haussener, C. Koval, J. S. Newman, J. W. Ager and R. A. Segalman, *Energy Environ. Sci.*, 2013, **7**, 297-301.
17.   A. J. Bard and L. R. Faulkner, *Electrochemical Methods, Fundamentals and Applications*, Wiley, 2000.
18.   Z. Samec, A. Trojanek and E. Samcova, *The Journal of Physical Chemistry*, 1994, **98**, 6352-6358.
19.   A. Herrera and H. Yeager, *Journal of The Electrochemical Society*, 1987, **134**, 2446-2451.
20.   K.-L. Huang, T. M. Holsen and J. R. Selman, *Industrial & engineering chemistry research*, 2003, **42**, 3620-3625.
21.   W. M. Deen, *Introduction to Chemical Engineering Fluid Mechanics*, Cambridge University Press, Cambridge, 2016.
22.   W. Sheng, Z. Zhuang, M. Gao, J. Zheng, J. G. Chen and Y. Yan, *Nature communications*, 2015, **6**.

23. A. Z. Weber, M. M. Mench, J. P. Meyers, P. N. Ross, J. T. Gostick and Q. Liu, *Journal of Applied Electrochemistry*, 2011, **41**, 1137.
24. H. F. Coward and G. W. Jones, *Limits of flammability of gases and vapors*, DTIC Document, 1952.
25. S. Y. Reece, J. A. Hamel, K. Sung, T. D. Jarvi, A. J. Esswein, J. J. H. Pijpers and D. G. Nocera, *Science*, 2011, **334**, 645-648.
26. S. Haussener, C. X. Xiang, J. M. Spurgeon, S. Ardo, N. S. Lewis and A. Z. Weber, *Energy Environ. Sci.*, 2012, **5**, 9922-9935.
27. C. X. Xiang, K. M. Papadantonakis and N. S. Lewis, *Mater Horiz*, 2016, **3**, 169-173.
28. J. Jin, K. Walczak, M. R. Singh, C. Karp, N. S. Lewis and C. X. Xiang, *Energ Environ Sci*, 2014, **7**, 3371-3380.
29. C. C. McCrory, S. Jung, I. M. Ferrer, S. Chatman, J. C. Peters and T. F. Jaramillo, *Journal of the American Chemical Society*, 2015.
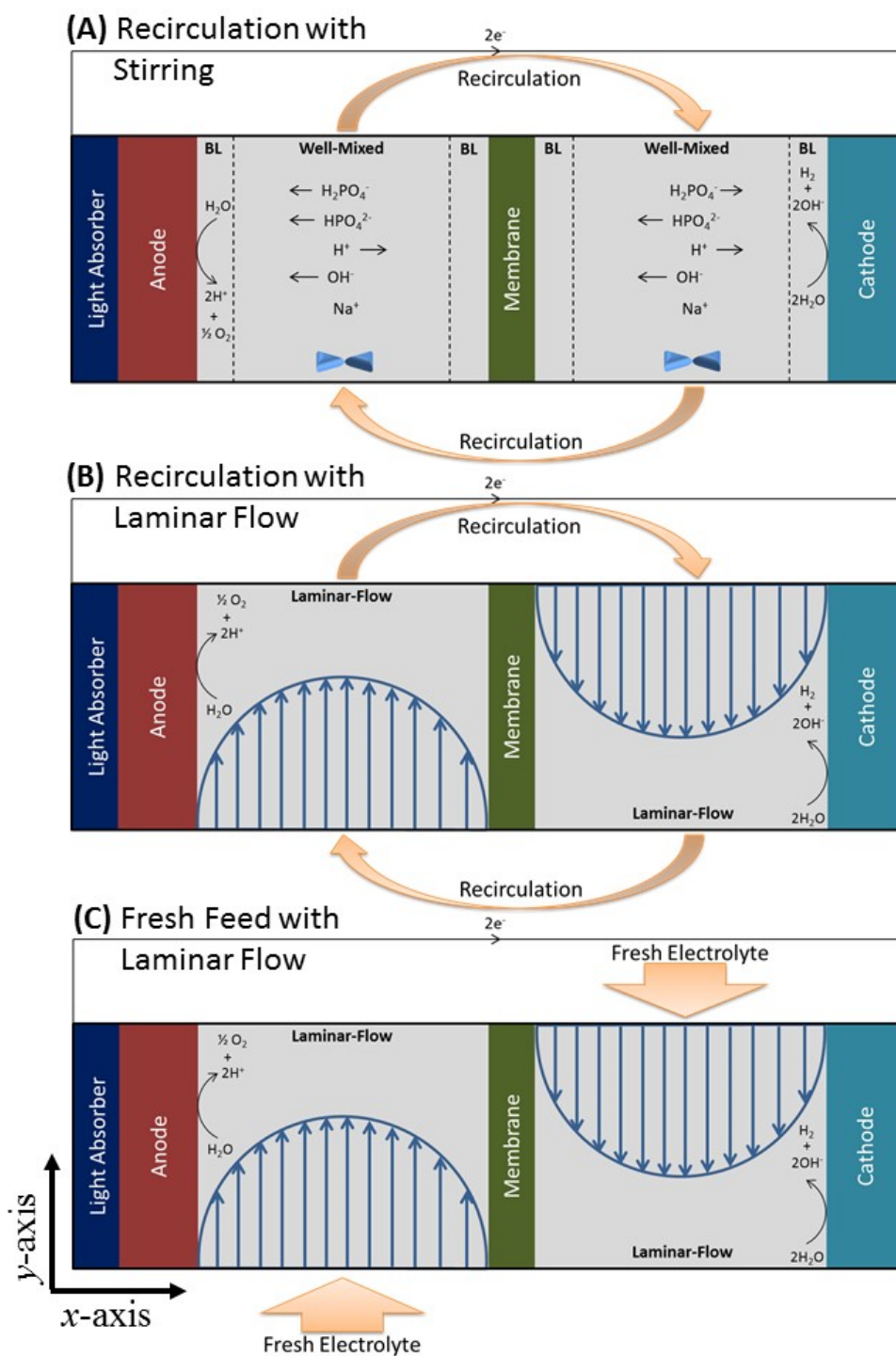
Figure 1. Schematic of three types of solar-driven water-splitting cells with different flow schemes. a) Recirculation cell with stirring; b) recirculation cell with laminar flow; and c) flow cell with a fresh laminar feed. Dimensions of cell are similar to those given in Ref [16]. The height of cell is 37 mm, width is 37 mm, the distance between membrane and electrode is 4 mm.
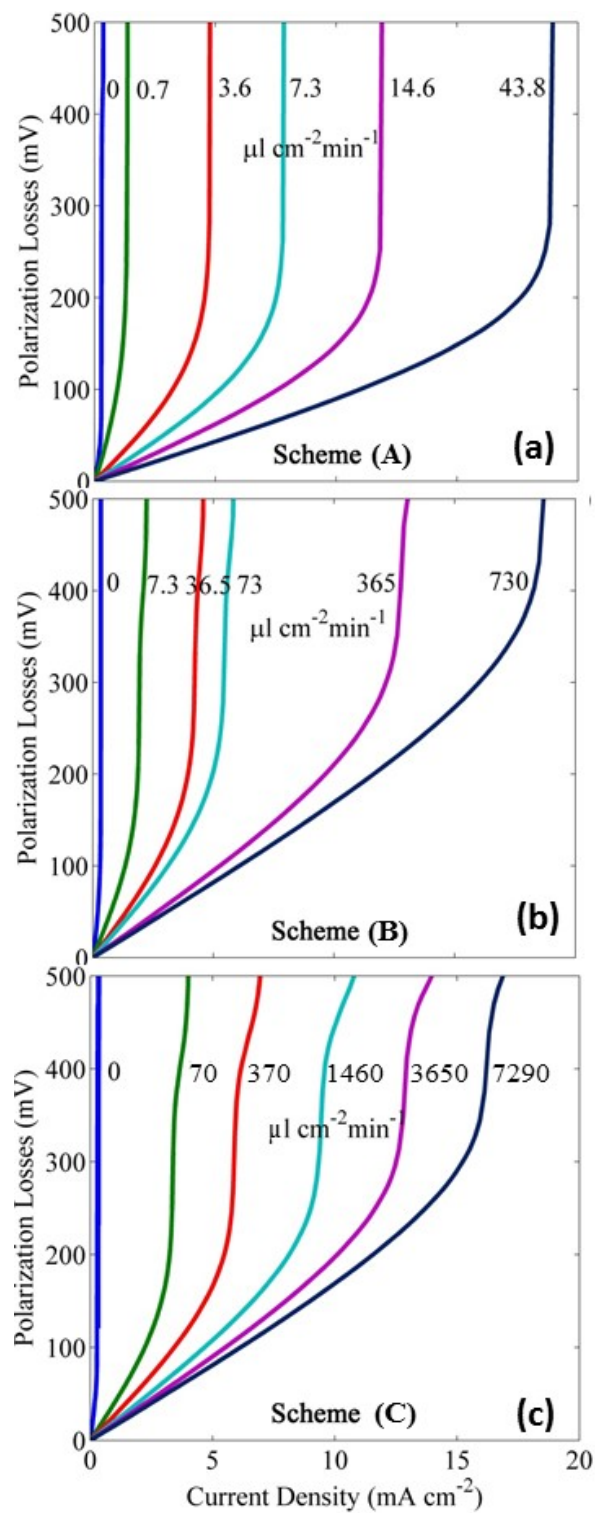
Figure 2. Polarization losses as a function of the operating current density in a 1-dimensional cell for (a) recirculation with stirring (Scheme A), (b) recirculation with laminar flow (Scheme B), and (c) fresh-feed electrolyte with laminar flow (Scheme C).
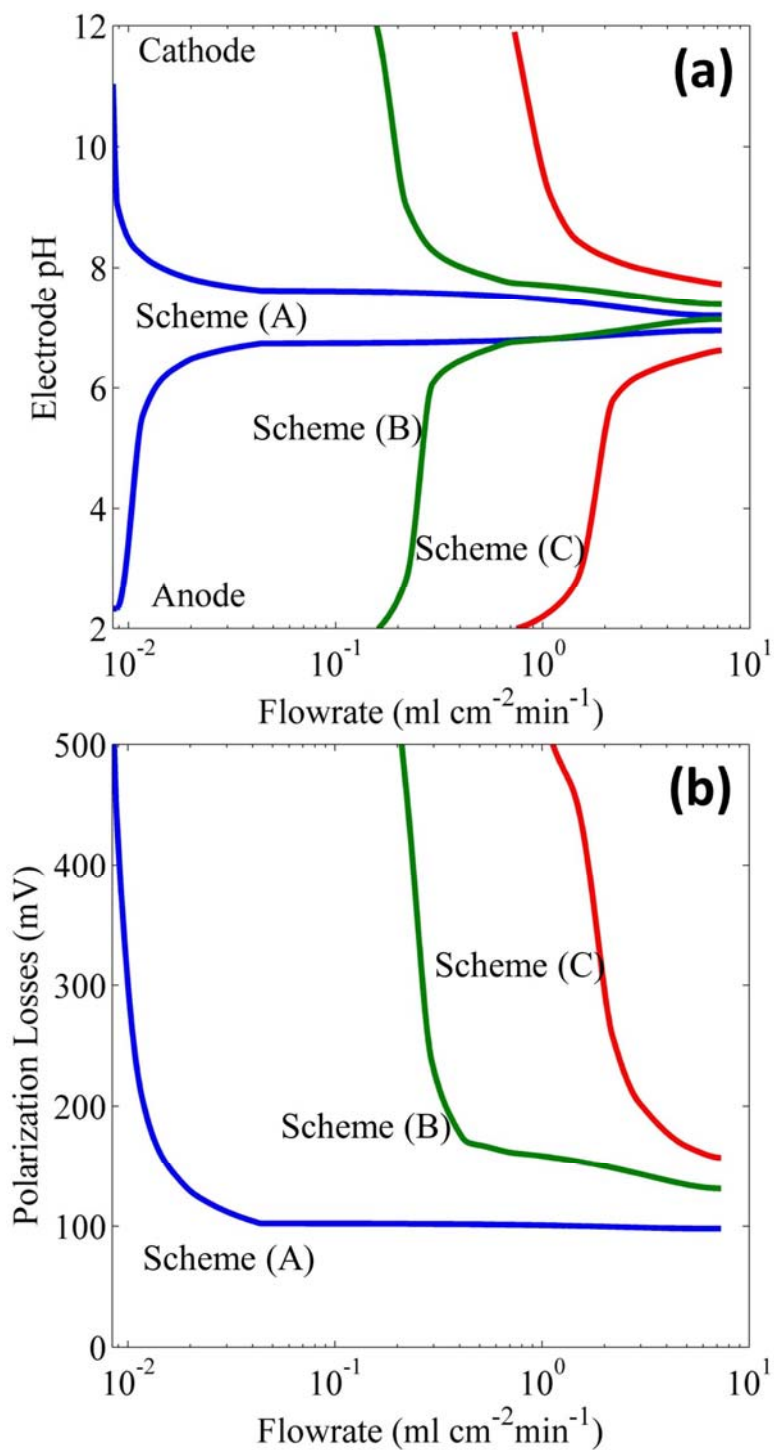
Figure 3. (a) The local pH at the surface of the electrode and (b) the total polarization loss surface as a function of the flow rate at an operating current density of 10 mA cm^{-2} in a 1-dimensional cell for recirculation cell with stirring (Scheme-A, blue), recirculation cell with laminar flow (Scheme-B, green), and flow cell with laminar flow (Scheme-C, red).
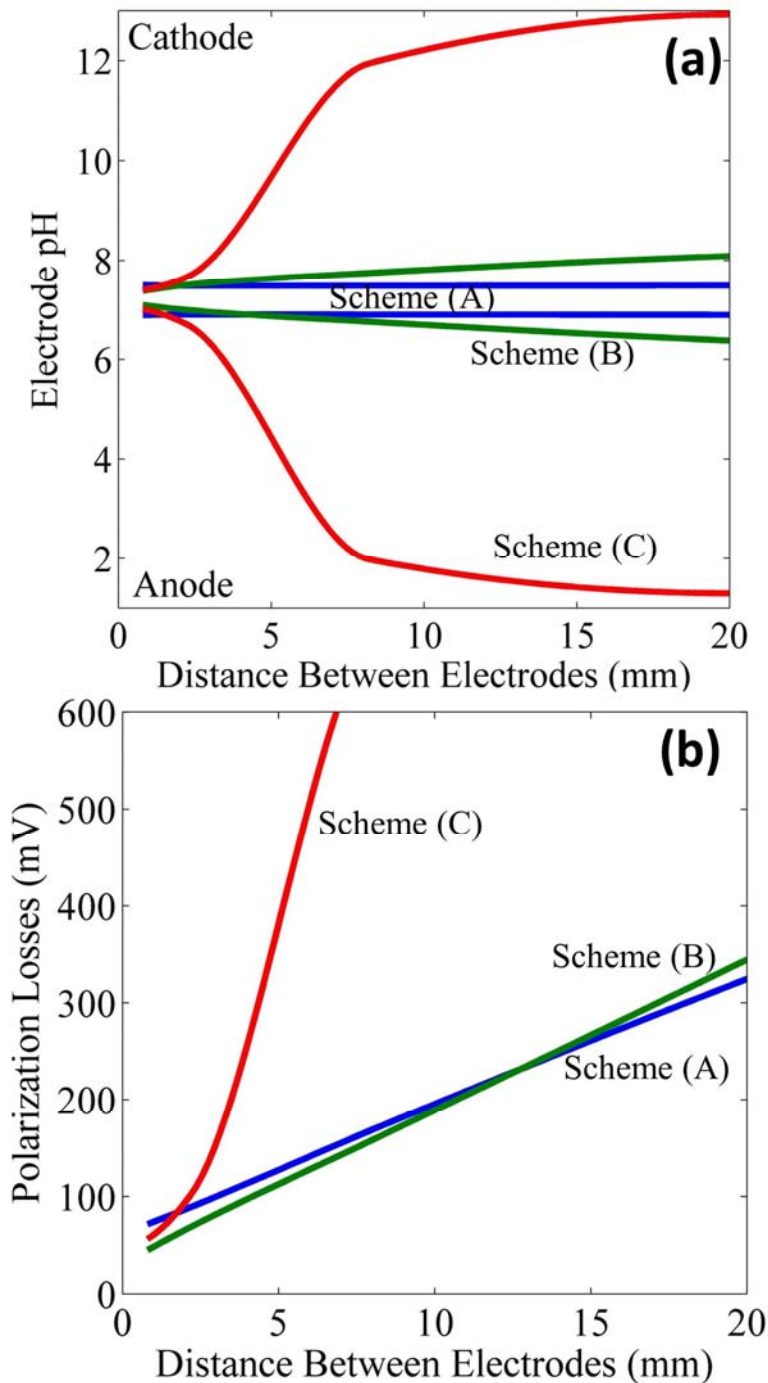
Figure 4: (a) The local pH at the surface of the electrode and (b) the total polarization loss as a function of the distance between the cathode and anode at an operating current density of 10 mA cm^{-2} for a recirculation cell with stirring (Scheme-A, blue), a recirculation cell with laminar flow (Scheme-B, green), and a flow cell with laminar flow (Scheme-C, red), each at a flow rate of 730 µl cm^{-2} min^{-1}.
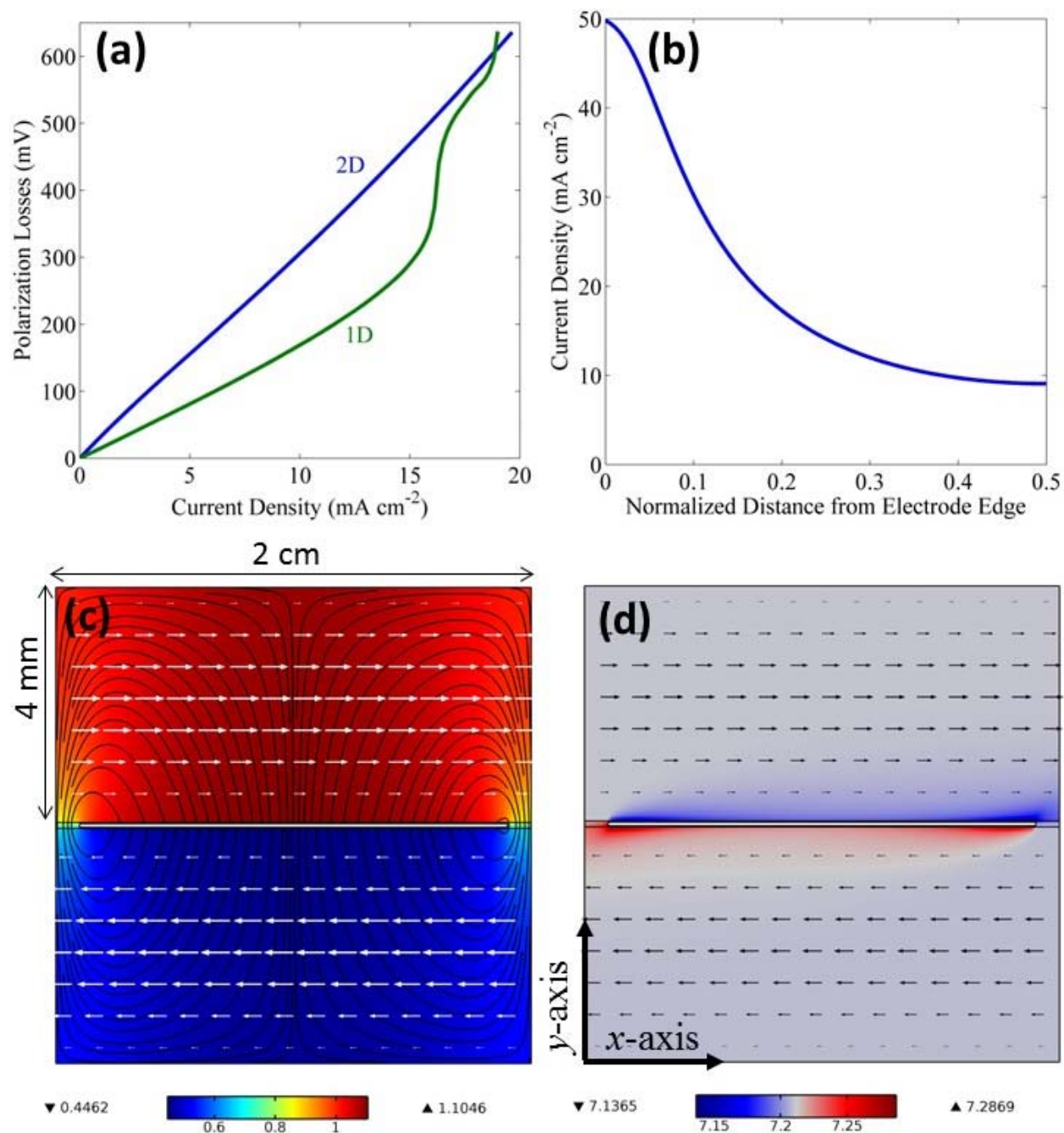
Figure 5: a) Polarization losses versus current density in 1D and 2D PECs operating with a fresh feed of pH 7.21 phosphate buffer at a flow rate of 7300 µl cm^{-2} min^{-1}, b) current density distribution at the photoelectrode-electrolyte interface, c) electrolyte potential distribution, and d) pH distribution in the 2D PEC cell at average current density of ~ 18 mA cm^{-2}. The counter-current velocity field is shown by the horizontal arrows.
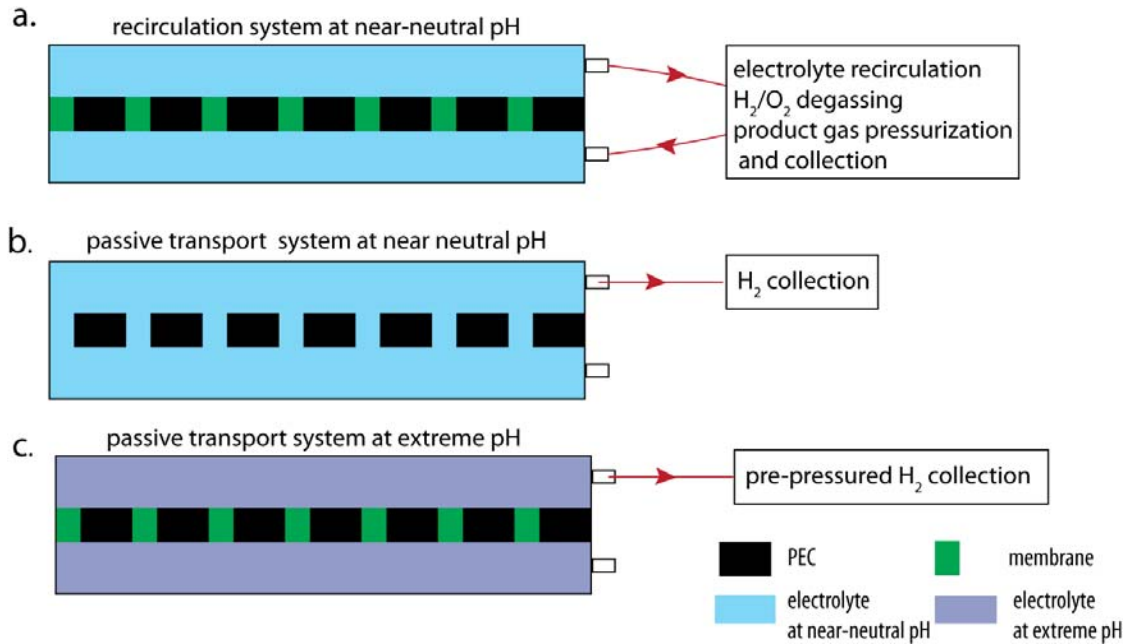
27

Figure 6: Schematic illustration of integrated PECs with a) a recirculation system at near-neutral pH with a membrane separator, b) a passive transport system at near-neutral pH without a membrane separator, and c) a passive transport system at extreme pH with a membrane separator.